

Xinyu HUI, Yingjie XU, Weihong ZHANG

Multiscale model of micro curing residual stress evolution in carbon fiber-reinforced thermoset polymer composites

© Higher Education Press 2020

Abstract In this study, the micro curing residual stresses of carbon fiber-reinforced thermoset polymer (CFRP) composites are evaluated using a multiscale modeling method. A thermochemical coupling model is developed at the macroscale level to obtain the distributions of temperature and degree of cure. Meanwhile, a representative volume element model of the composites is established at the microscale level. By introducing the information from the macroscale perspective, the curing residual stresses are calculated using the microscale model. The evolution of curing residual stresses reveals the interaction mechanism of fiber, matrix, and interphase period during the curing process. Results show that the curing residual stresses mostly present a tensile state in the matrix and a compressive state in the fiber. Furthermore, the curing residual stresses at different locations in the composites are calculated and discussed. Simulation results provide an important guideline for the analysis and design of CFRP composite structures.

Keywords CFRP, curing residual stress, multiscale modeling, finite element method

1 Introduction

Carbon fiber-reinforced thermoset polymer (CFRP) composites have been widely used in various applications, such as aeronautics and aerospace, automotive, and marine and

civil engineering, due to its high specific stiffness and strength [1–3]. The autoclave curing process is a commonly used method in the manufacturing of CFRP composite parts of different industries [4,5]. In the curing process, the residual stresses invariably occur due to the mismatched thermal expansion between the fiber and matrix and the chemical shrinkage of the matrix. Curing residual stress is a critical defect that affects the mechanical performance of composite parts. For instance, the release of residual stresses results in shape distortion, that is, curing deformation [6]. In extreme cases, large residual stresses can even cause debonding in the fiber–matrix interphase and microcracks in the matrix before loading [7]. Therefore, investigating the evolution of curing residual stresses is important to understand the mechanical performance of final composite parts thoroughly.

Several experimental methodologies have been used to measure the curing residual stresses in CFRP composites. For example, strain gauges [8,9] or fiber optic sensors [10] were embedded in composites to characterize the evolution of residual stresses in curing processes. Destructive methods, including hole drilling [11] and indentation [12] methods, have also been used to characterize the final residual stresses of cured composite parts. However, experimental methods are usually complicated and costly to monitor the evolution of residual stresses during curing. Moreover, experimental methods cannot capture the curing residual stresses developed at the microscale level, that is, the residual stresses in the fiber–matrix interphase.

Therefore, many studies have focused on investigating curing residual stresses numerically [13–15]. The generation of curing residual stresses is a complicated cure reaction of process coupling, heat transfer, and mechanical response. Many researchers have presented various cure kinetics models, such as N-order [16] and Kamal [17] models, to characterize the cure reaction process. The temperature of composites in the curing process is affected by the applied temperature boundary in the autoclave, heat transfer in the mold, and heat released in the cure reaction. Thus, thermochemical simulations have been widely used

Received January 8, 2020; accepted March 20, 2020

Xinyu HUI, Yingjie XU (✉), Weihong ZHANG
State IJR Center of Aerospace Design and Additive Manufacturing,
School of Mechanical Engineering, Northwestern Polytechnical
University, Xi'an 710072, China
E-mail: xu.yingjie@nwpu.edu.cn

Yingjie XU
Shaanxi Engineering Laboratory of Aerospace Structure Design and
Application, School of Mechanical Engineering, Northwestern
Polytechnical University, Xi'an 710072, China

to capture the temperature and degree of cure variations in composites during the curing processes [18]. Curing residual stresses can be further calculated via thermo-mechanical analysis based on the obtained temperature fields and degree of cure. The characterization of curing residual stresses can be presented from macro- [19–21] to microscale [22–25]. However, macro residual stresses cannot intuitively reflect stress distributions in the different phases (fiber, matrix, and interphase) of composites. In this case, an increasing number of investigations has focused on the prediction of micro residual stresses by using the micromechanics method [26,27]. The representative volume element (RVE) is usually modeled in accordance with the periodic structure of composites, and finite element simulation is used to predict the residual stresses.

Although these studies have been conducted to investigate the micro curing residual stresses of composites, most have neglected the effects of interphase on micro curing residual stresses. Meanwhile, studies on the evolution of micro curing residual stresses at various locations in the composites are limited. In the composites of carbon fiber-reinforced resin matrices, the interphase is a three-dimensional, heterogeneous, and transitive region where the two components (fiber and matrix) meet [28]. As shown in Fig. 1, Qi et al. [28] presented the interphase in the composites of carbon fiber-reinforced resin matrices via atomic force microscopy. Thus, this study aims to present a detailed investigation of micro curing residual stresses by using a multiscale modeling method. The temperature and degree of cure are first obtained via macroscale thermochemical simulation. Then, in consideration of the interphase, an RVE model of the composites is developed. The macroscale simulation result is then introduced into the microscale RVE model to calculate the micro curing residual stresses. The evolution of micro curing residual stresses in various phases (fiber, matrix, and interphase) and locations (along the thickness) is calculated and discussed in detail.

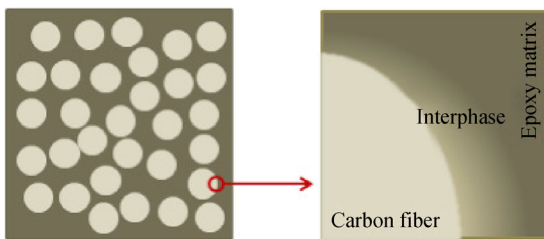


Fig. 1 Atomic force microscope observation of the interphase. Reprinted with permission from Ref. [28] from Elsevier.

2 Multiscale modeling framework and theoretical formulation

The composite system T300/5228 in this study is commonly used in aeronautical structures. The multiscale

modeling framework shown in Fig. 2 is proposed to predict the micro curing residual stresses of composites. The following steps are involved in this framework:

1) At the macroscale, the temperature and degree of cure of composites in the curing process are calculated via coupled thermochemical analysis. A three-dimensional heat transfer problem considering the heat released via curing reaction is solved.

2) The calculated temperature and degree of cure in the macroscale model are further imposed in the microscale RVE to predict the curing residual stresses. The constitutive models of fiber, interphase, and matrix are defined.

2.1 Macroscale model

2.1.1 Heat transfer equation

The temperature field of composites depends on the external curing temperature profile and the heat released by the curing reaction of resin and is considered a nonlinear temperature transfer problem with heat source. The three-dimensional heat transfer equation of composites during a curing process can be expressed as follows [29]:

$$\rho C \frac{\partial T}{\partial t} = k_{xx} \frac{\partial^2 T}{\partial x^2} + k_{yy} \frac{\partial^2 T}{\partial y^2} + k_{zz} \frac{\partial^2 T}{\partial z^2} + \dot{q}, \quad (1)$$

where T is the current temperature, t is the curing reaction time, C and ρ are the specific heat and density of composites, respectively, and k_{xx} , k_{yy} , and k_{zz} are the thermal conductivities of the composites in the three directions. The density of the T300/5228 prepreg is provided by the supplier. The thermal conductivities and specific heat of the T300/5228 composite system are tested and listed below:

$$k_{xx} = 5.1309 + 0.01876T \text{ W} \cdot \text{m}/^\circ\text{C};$$

$$k_{yy} = k_{zz} = 0.6522 + 0.0017T \text{ W} \cdot \text{m}/^\circ\text{C};$$

$$C = 1.154 \text{ J}/(\text{g} \cdot ^\circ\text{C});$$

$$\rho = 1540 \text{ kg}/\text{m}^3.$$

The following rate of heat generation \dot{q} in Eq. (1) is related to the curing reaction of resin matrices in composites:

$$\dot{q} = \rho_r (1 - V_f) H_r \frac{d\alpha}{dt}, \quad (2)$$

where ρ_r is the density of the resin, V_f is the fiber volume fraction, H_r is the total heat released by the curing reaction of a unit mass of resin, α is the degree of cure of the resin; and $\frac{d\alpha}{dt}$ is the resin's instantaneous curing rate, which can be determined through the cure kinetics model.

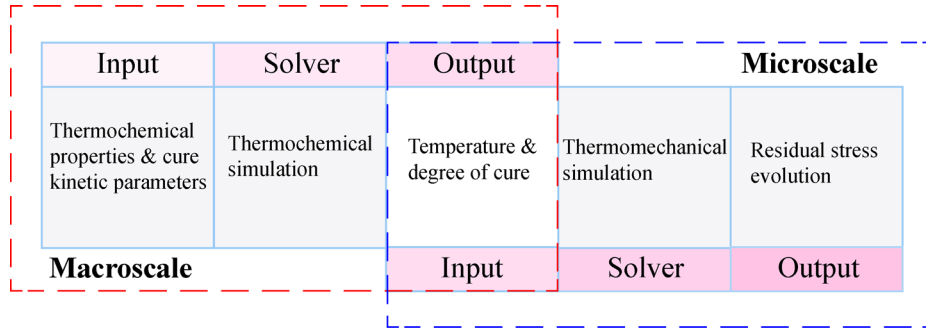


Fig. 2 Illustration of the multiscale modeling framework.

2.1.2 Cure kinetics equation

In this study, a differential scanning calorimetry (DSC) test is conducted to characterize the curing reaction kinetics of 5228 epoxy resin. On the basis of the DSC test results, the cure kinetics model can be derived to describe the relationship between the curing rate with temperature and the degree of cure during the curing process. In this study, the following phenomenological framework [17] is used to model the cure kinetics of resin:

$$\frac{d\alpha}{dt} = (K_1 + K_2\alpha^m)(1-\alpha)^n, \quad (3)$$

where m and n are the reaction orders, and K_1 and K_2 are the constants of reaction rate governed by Arrhenius equations. These constants can be expressed as follows:

$$K_i = A_i \exp\left(\frac{-\Delta E_i}{RT}\right), \quad i = 1, 2, \quad (4)$$

where A_i is the pre-exponential factor, E_i is the reaction activation energy, and R is the universal gas constant. The parameter values of the cure kinetics model are calibrated using the DSC test results listed below:

$$\begin{aligned} A_1 &= 1269.65 \text{ s}^{-1}; \\ A_2 &= 438948.12 \text{ s}^{-1}; \\ m &= 0.046; \\ n &= 1.095; \\ E_1 &= 7036.32 \text{ J/mol}; \\ E_2 &= 9761.48 \text{ J/mol}; \\ R &= 8.3145. \end{aligned}$$

2.1.3 Coupled thermochemical simulation

Coupled thermochemical analysis is conducted using the commercial software package ABAQUS to calculate the temperature distribution and degree of cure. In this study, a cross-ply plate made of four symmetric plies [0/90/90/0] with dimensions of 100 mm × 100 mm × 30 mm is considered. User subroutines UMATHT and USEFLD are written in ABAQUS to implement the coupled thermo-

chemical simulation. The finite element model of the composite plate is shown in Fig. 3. Eight-node linear heat transfer (DC3D8) elements of ABAQUS are used.

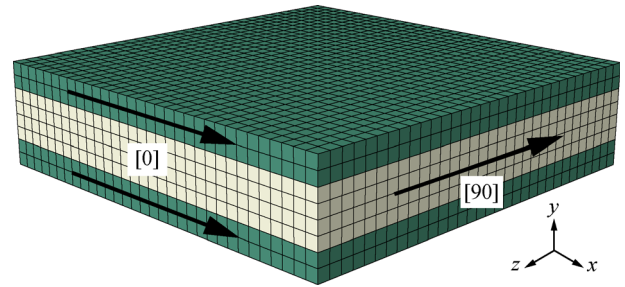


Fig. 3 Finite element model of the macroscale composite plate.

2.2 Microscale model

2.2.1 Constitutive models of fiber, interphase, and resin

At the microscale level, each phase of the composites exhibits different constitutive behavior during the curing process. The elastic and thermal properties of the fiber and interphase are all considered constant during the curing process. The mechanical properties including thermal expansion of the T300 fiber and interphase in Refs. [30,31] are used. By contrast, the constitutive behavior of resin remarkably varies with the degree of cure during the curing process. In this study, the elastic behavior of resin during the curing process is described using an incrementally linear elasticity model [32,33]. The total strain increment of resin is described as follows:

$$\Delta\boldsymbol{\varepsilon} = \Delta\boldsymbol{\varepsilon}^e + \Delta\boldsymbol{\varepsilon}^{\text{th}} + \Delta\boldsymbol{\varepsilon}^{\text{ch}}, \quad (5)$$

where $\Delta\boldsymbol{\varepsilon}^e$, $\Delta\boldsymbol{\varepsilon}^{\text{th}}$, and $\Delta\boldsymbol{\varepsilon}^{\text{ch}}$ are the elastic strain, thermal strain, and chemical shrinkage increments, respectively. Chemical shrinkage occurs in the 5228 resin after the gel point at 0.6% [13].

The equivalent stress increment can be expressed as follows:

$$\Delta\sigma = C\Delta\varepsilon, \quad (6)$$

where C is the elastic matrix. In this study, the variation in the elastic properties of resin during the curing process is described as follows [34]:

$$E = \begin{cases} E^0 & \alpha < \alpha_{\text{gel}}, \\ (1 - \alpha_{\text{mod}})E^0 + \alpha_{\text{mod}}E^\infty & \alpha \geq \alpha_{\text{gel}}, \end{cases} \quad (7)$$

where α_{gel} is the degree of cure at the gel point, which is determined as 0.4 by the DSC test [14]. α_{mod} is considered the function of degree of cure and the gel point and is calculated as follows:

$$\alpha_{\text{mod}} = \frac{\alpha - \alpha_{\text{gel}}}{1 - \alpha_{\text{gel}}}. \quad (8)$$

E^0 and E^∞ denote the moduli of uncured and cured resin, where E^0 can be derived from the following equations:

$$\begin{cases} K^0 \approx K^\infty/2.5, \\ G^0 \approx G^\infty/100, \\ \nu^0 = (3K^0 - 2G^0)/(6K^0 + 2G^0), \\ E^0 = 2(1 + \nu^0)G^0, \end{cases} \quad (9)$$

where K is bulk modulus, G is shear modulus, and ν is Poisson's ratio. The variation in the thermal expansion coefficient (CTE) of resin during the curing process is expressed as follows [35]:

$$\beta = (1 - \alpha)\beta_r + \alpha\beta_g, \quad (10)$$

where β_r and β_g are the thermal expansion coefficients of resin in rubbery and viscous flow (uncured) and glassy (cured) states, respectively. In accordance with the test results of the elastic moduli and the thermal expansion coefficients of uncured and cured resin, the parameters in Eqs. (8)–(10) are listed below:

Fiber: $E_1 = 233$ GPa, $E_2 = E_3 = 23.1$ GPa, $G_{12} = G_{13} = 8.96$ GPa, $G_{23} = 8.26$ GPa, $\nu_{12} = \nu_{13} = 0.2$, $\nu_{23} = 0.398$, $CTE_1 = -0.54 \times 10^{-6} \text{ }^\circ\text{C}^{-1}$, $CTE_2 = CTE_3 = 10.1 \times 10^{-6} \text{ }^\circ\text{C}^{-1}$;

Interphase: $E = 10.2$ GPa, $\nu = 0.28$, $CTE = 20 \times 10^{-6} \text{ }^\circ\text{C}^{-1}$;

Matrix: $E^0 = 20.8$ MPa, $E^\infty = 3.483$ GPa, $\nu^0 = 0.49$, $\nu^\infty = 0.336$, $\beta_r = 35.36 \times 10^{-6} \text{ }^\circ\text{C}^{-1}$, $\beta_g = 88.4 \times 10^{-6} \text{ }^\circ\text{C}^{-1}$.

2.2.2 Computation of micro curing residual stresses

The micro curing residual stresses are evaluated using the microscale RVE model with square fiber arrangement, as

shown in Fig. 4. The RVE model consists of an 8 μm -diameter fiber, 0.1 μm -thick interphase, and resin matrix. The fiber volume fraction is 53%. The finite element mesh is implemented with 155500 eight-node linear break elements (C3D8) in ABAQUS.

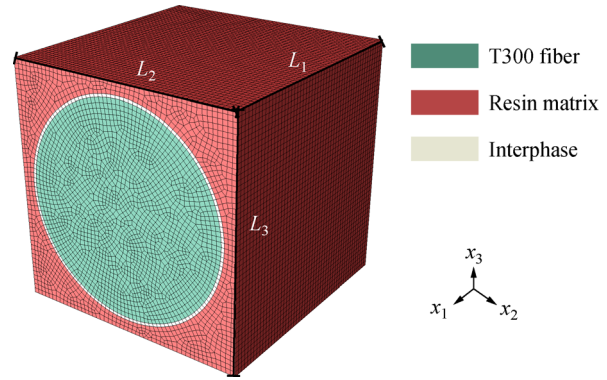


Fig. 4 Finite element model of the microscale RVE.

A user subroutine UMAT is written to describe the constitutive behavior of each phase in the microscale model. The properties of resin are updated in accordance with the simulation result of the degree of cure from the macroscale model. The calculated temperatures from the macroscale model are imposed on the microscale RVE model to predict the curing residual stress via coupled thermomechanical analysis. Periodical boundary conditions [36] are applied to the RVE model. In addition, 0.6 MPa pressure loads are imposed on the external surface of the model to simulate an actual pressure environment in the autoclave system. Three-dimensional periodical boundary conditions [36] are applied to the RVE model and expressed as follows:

$$\begin{cases} U_1(L_1, x_2, x_3) - U_1(0, x_2, x_3) = L_1\varepsilon_{11}, \\ U_2(L_1, x_2, x_3) - U_2(0, x_2, x_3) = 2L_2\varepsilon_{12}, \\ U_3(L_1, x_2, x_3) - U_3(0, x_2, x_3) = 2L_3\varepsilon_{13}, \\ U_1(x_1, L_2, x_3) - U_1(x_1, 0, x_3) = 2L_1\varepsilon_{22}, \\ U_2(x_1, L_2, x_3) - U_2(x_1, 0, x_3) = L_2\varepsilon_{22}, \\ U_3(x_1, L_2, x_3) - U_3(x_1, 0, x_3) = 3L_3\varepsilon_{32}, \\ U_1(x_1, x_2, L_3) - U_1(x_1, x_2, 0) = 2L_1\varepsilon_{33}, \\ U_2(x_1, x_2, L_3) - U_2(x_1, x_2, 0) = 2L_2\varepsilon_{32}, \\ U_3(x_1, x_2, L_3) - U_3(x_1, x_2, 0) = L_3\varepsilon_{33}, \end{cases} \quad (11)$$

where L_i ($i = 1, 2, 3$) and U_i ($i = 1, 2, 3$) represent the lengths and displacements of the microscale RVE, respectively, along the x_1 , x_2 , and x_3 directions, and ε_{ij} are the tensorial strains.

3 Results and discussion

3.1 Evolution of temperature and degree of cure

The macroscale model is subjected to a prescribed temperature profile. The temperature profile with two heat preservation platforms is described as follows: First, the temperature is initially set to 25 °C and then increased to 120 °C with a heating rate of 3 °C/min. Second, a short heat preservation (first dwelling) platform is carried out for 1 h, and the temperature is increased to 180 °C with the same heating rate. Third, a long heat preservation platform (second dwelling) is carried out for 150 min to provide sufficient curing. Finally, the temperature is decreased to 25 °C with a cooling rate of -3 °C/min.

The temperature distribution on the macroscale composite plate after cooling is presented in Fig. 5. The temperature difference in the composite is evident. Given that the lower layer of the composite plate adheres to the mold during the curing process, the temperature value determined by the curing temperature history is set in the lower surface of the model. In the other surface, convective boundary conditions are assigned. When the curing

reaction is completed, the temperature in the upper layer is higher than that in the lower layer, and the maximum difference is 13.4 °C.

Figure 6 presents the history of temperature and degree of cure at the central point of the macroscale model. In the first stage of heat preservation, resin is solidified slowly. At the beginning of the second dwelling period, the resin begins to cure rapidly, accompanied by an increase in internal temperature (higher than the applied temperature) and a significant increase in the degree of cure. During the second dwelling period, the resin is almost fully cured with a constant degree of cure.

3.2 Evolution of micro curing residual stresses

After macroscale modeling, the degree of cure and temperature at all the nodes of the macroscale model are obtained. Then, the results at the central node of the macroscale model are transferred to the microscale model to characterize the micro curing residual stresses further. The distributions of micro curing residual stresses of the microscale model after curing are depicted in Fig. 7, where S11 represents the fiber direction.

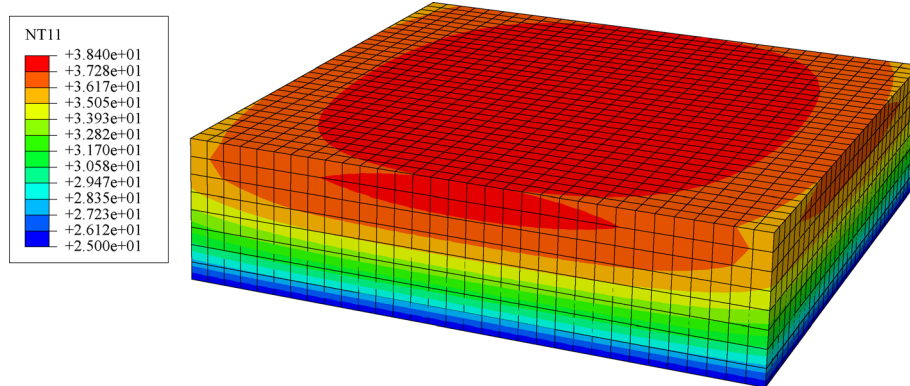


Fig. 5 Temperature distribution in the macroscale model after the curing cycle.

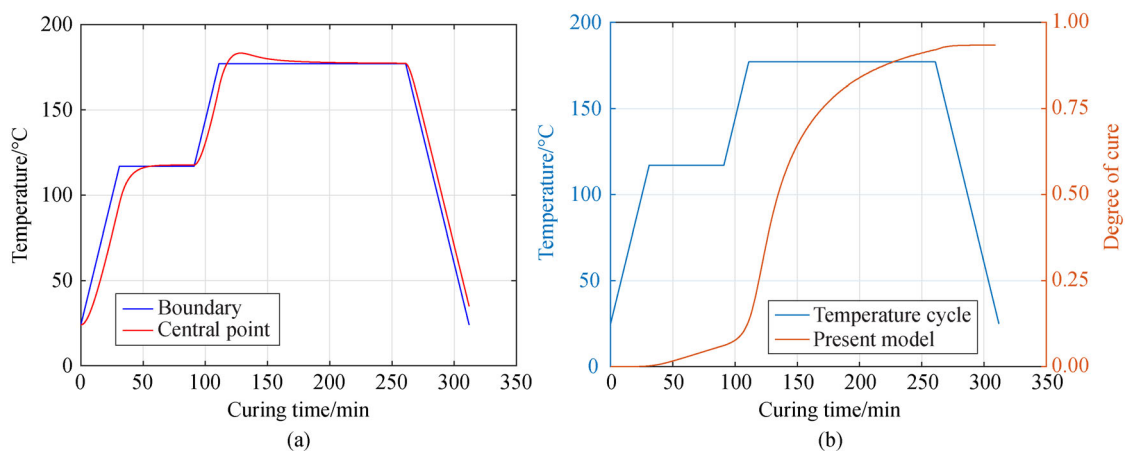


Fig. 6 Evolution of (a) temperature and (b) degree of cure with curing time.

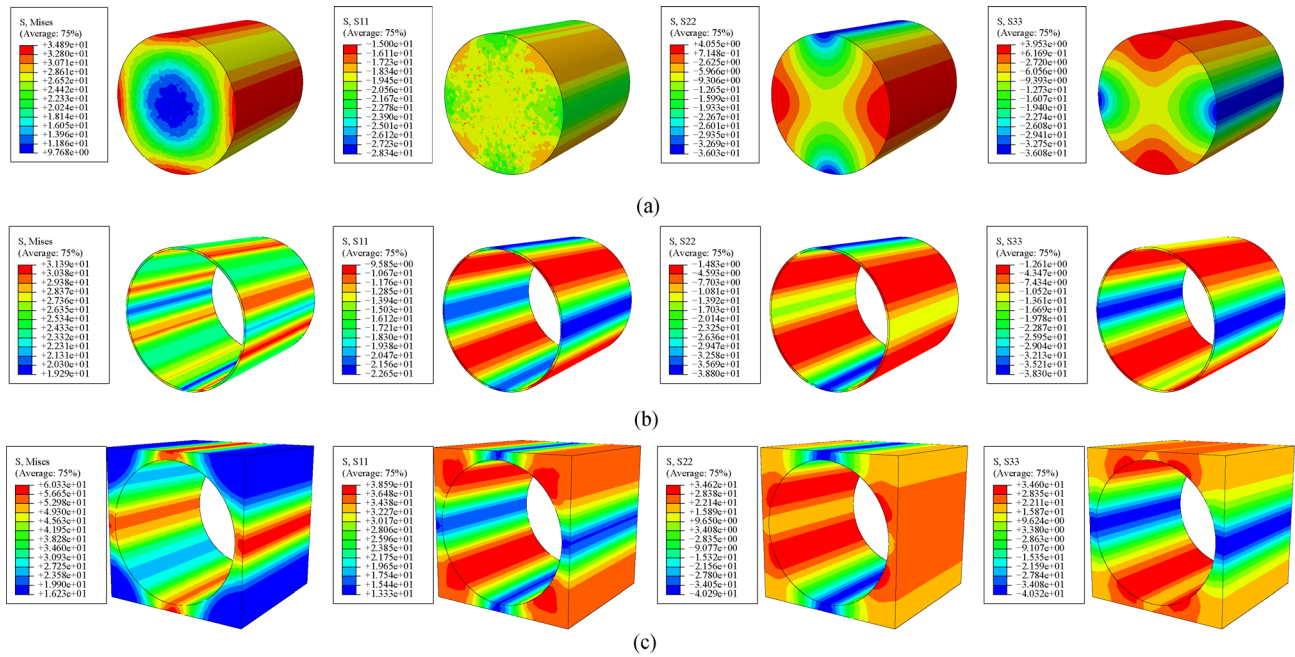


Fig. 7 Distributions of the curing residual stresses of the microscale model after the curing cycle in the (a) fiber, (b) the interphase, and (c) the matrix.

After curing, compressive residual stresses in three directions occur in the interphase. In the fiber, the curing residual stresses along the fiber direction (S11) are all compressive. Along the transverse directions (S22 and S33), most of the curing residual stresses are under the compressive state, whereas a small portion of the stresses is under the tensile state. Compared with that of fiber, the curing residual stresses in the matrix shows an opposite distribution. The curing residual stresses along the S11 direction undergo a completely tensile state. Along the S22 and S33 directions, most of the curing residual stresses are under the tensile state, whereas a small portion of the stresses is under the compressive state.

The evolution of the maximum von Mises curing residual stresses is plotted in Fig. 8. Figure 8(a) shows that the evolution of curing residual stresses in resin undergoes several stages. Before reaching its gel point, the resin's residual stresses are significantly low due to its small modulus. The increase in temperature gradually increases the curing degree of resin, and chemical shrinkage occurs as the resin reaches its gel point. Chemical shrinkage leads to the rapid increase in the curing of residual stresses, as shown in Fig. 8(a). Then, the curing residual stresses maintain a stable value in the second heat preservation platform. During the cooling stage, the residual stresses increase sharply due to the large temperature difference. The coefficient of thermal expansion in fiber is clearly lower than that of resin. Thus, the generation of residual stresses in fiber is mainly from the influence of resin deformation. Therefore, the evolution law of curing residual stresses in fiber is similar to that of

the resin matrix, as shown in Fig. 8(b). By contrast, the generation of residual stress in the interphase is mainly due to its thermal deformation during the curing process. Thus, the evolution law of curing residual stresses is generally consistent with the temperature curve, as shown in Fig. 8(c).

3.3 Micro curing residual stresses at different locations

In practice, the evolution of curing residual stresses in a composite part varies with different locations, especially along the thickness direction. In the macroscale model in this study, five reference points at different locations along the thickness direction (Fig. 9) are considered.

The temperature and degree of cure evolution at the reference points are first calculated via coupled thermo-chemical analysis. Given that the evolution laws at the five reference points have almost the same behavior, only the temperature and degree of cure at the end of curing are presented in this study. As shown in Fig. 10, the temperature and degree of cure increase along the thickness direction. Given that the temperature in the upper layer is higher than that in the lower layer, the curing reaction of the resin matrix located in the upper layer is more complete. The temperature and degree of cure at Points 1 and 5 are 25 °C and 0.925, and 37 °C and 0.936, respectively.

The von Mises curing residual stresses at the reference points are presented in Fig. 11. The curing residual stresses slightly decrease along the thickness direction due to the temperature distribution along the thickness direction. At

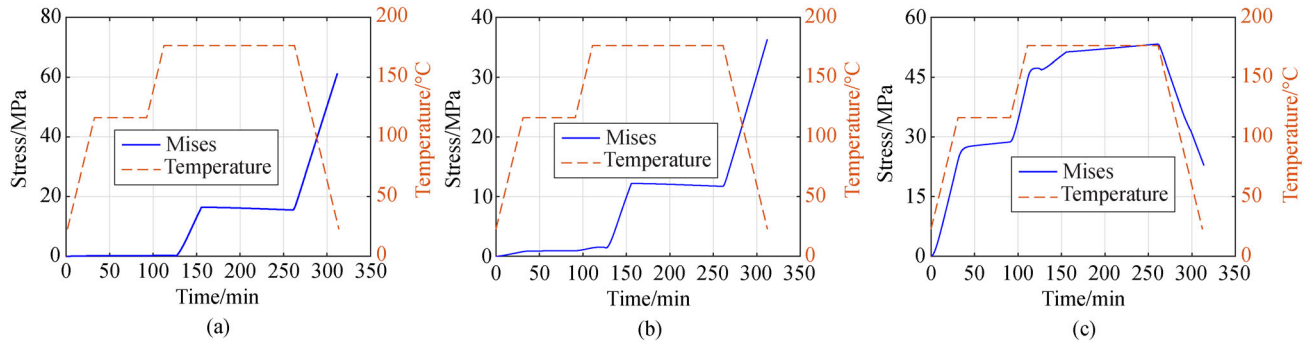


Fig. 8 Evolution of curing residual stresses in the (a) matrix, (b) fiber, and (c) interphase.

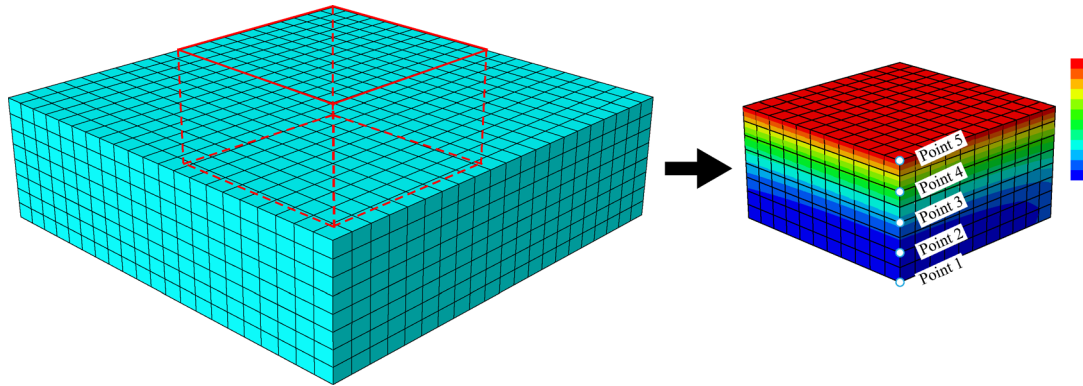


Fig. 9 Illustration of the five reference points at different locations in the macroscale model.

the end of curing, the temperature difference in the upper surface is lower than that in the lower surface; thus, lower residual stresses are found at the upper surface.

4 Conclusions

A multiscale modeling method is proposed to investigate the micro curing residual stresses of CFRP composites. This method effectively achieves information transmission, such as that of temperature and degree of cure between different scales. In the process of solving the curing residual stresses, the material property evolution and chemical shrinkage of resin are considered. Through micromechanical analysis, the coupled thermomechanical behavior of the fiber, interphase, and matrix during curing are characterized. The contour plot of the residual stresses of the microscale model demonstrates a tensile state in the matrix and a compressive state in the fiber and interphase of the curing residual stresses. Furthermore, the evolution laws of the curing residual stresses in the fiber, interphase, and matrix are discussed in detail. Several reference points along the thickness direction of the macroscale model are selected to calculate the curing residual stresses. The results show that the curing residual stresses decrease along the thickness direction.

Experimental verification is not conducted in this study. The curing residual stresses at the microscale level are difficult to obtain with existing experimental methods. Nevertheless, curing deformation induced by the curing residual stresses can be tested easily. Therefore, in future studies, the curing deformation of composite samples will be computed using the curing residual stresses. At present, we use this simplified RVE model to develop the

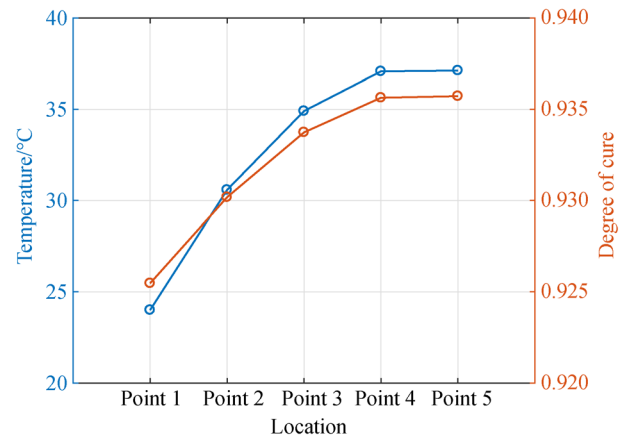


Fig. 10 Temperature and degree of cure at the reference points after curing.

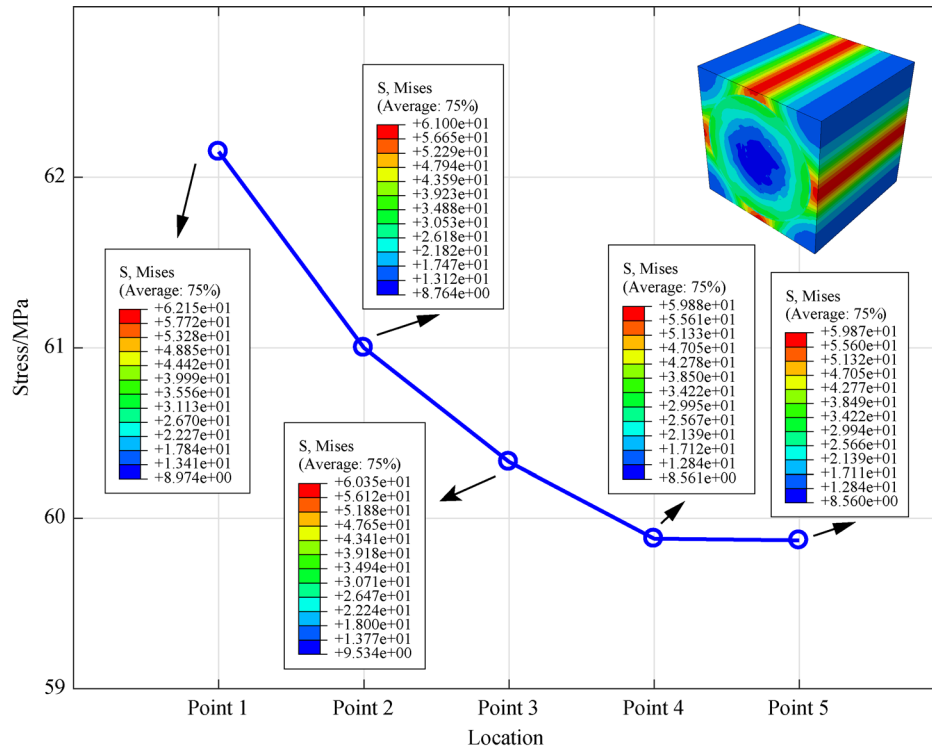


Fig. 11 Curing residual stresses at the reference points after curing.

multiscale modeling method. This multiscale modeling method will be further improved with a refined RVE model that contains multifiber.

Acknowledgements This work was supported by the National Key Research and Development Program of China (Grant No. 2017YFB1102800) and the National Natural Science Foundation of China (Grant Nos. 11872310 and 51761145111).

References

- Geier N, Davim J P, Szalay T. Advanced cutting tools and technologies for drilling carbon fibre reinforced polymer (CFRP) composites: A review. *Composites Part A: Applied Science and Manufacturing*, 2019, 125: 105552
- Vigneshwaran S, Uthayakumar M, Arumugaprabu V. Review on machinability of fiber reinforced polymers: A drilling approach. *Silicon*, 2018, 10(5): 2295–2305
- Kovács L, Romhány G. Derivation of ply specific stiffness parameters of fiber reinforced polymer laminates via inverse solution of classical laminate theory. *Periodica Polytechnica Mechanical Engineering*, 2018, 62(2): 158–164
- Streitferdt A, Rudolph N, Taha I. Co-curing of CFRP-steel hybrid joints using the vacuum assisted resin infusion process. *Applied Composite Materials*, 2017, 24(5): 1137–1149
- Ho Y C, Yanagimoto J. Effect of unidirectional prepreg size on punching of pseudo-ductile CFRP laminates and CFRP/metal hybrid composites. *Composite Structures*, 2018, 186: 246–255
- Bellini C, Sorrentino L. Analysis of cure induced deformation of CFRP U-shaped laminates. *Composite Structures*, 2018, 197: 1–9
- Danzi F, Fanteria D, Panettieri E, et al. A numerical micro-mechanical study on damage induced by the curing process in carbon/epoxy unidirectional material. *Composite Structures*, 2019, 210: 755–766
- Zhang K, Yang Z, Li Y. A method for predicting the curing residual stress for CFRP/Al adhesive single-lap joints. *International Journal of Adhesion and Adhesives*, 2013, 46: 7–13
- Ghasemi A R, Mohammadi M M. Residual stress measurement of fiber metal laminates using incremental hole-drilling technique in consideration of the integral method. *International Journal of Mechanical Sciences*, 2016, 114: 246–256
- Okabe Y, Yashiro S, Tsuji R, et al. Effect of thermal residual stress on the reflection spectrum from fiber Bragg grating sensors embedded in CFRP laminates. *Composites Part A: Applied Science and Manufacturing*, 2002, 33(7): 991–999
- Bateman M G, Miller O H, Palmer T J, et al. Measurement of residual stress in thick section composite laminates using the deep-hole method. *International Journal of Mechanical Sciences*, 2005, 47(11): 1718–1739
- Nishikawa M, Soyama H. Two-step method to evaluate equibiaxial residual stress of metal surface based on micro-indentation tests. *Materials & Design*, 2011, 32(6): 3240–3247
- Ersoy N, Tugutlu M. Cure kinetics modeling and cure shrinkage behavior of a thermosetting composite. *Polymer Engineering and Science*, 2010, 50(1): 84–92
- Kravchenko O G, Kravchenko S G, Pipes R B. Chemical and thermal shrinkage in thermosetting prepreg. *Composites Part A: Applied Science and Manufacturing*, 2016, 80: 72–81

15. Okabe T, Takehara T, Inose K, et al. Curing reaction of epoxy resin composed of mixed base resin and curing agent: Experiments and molecular simulation. *Polymer*, 2013, 54(17): 4660–4668
16. Turi E A. *Thermal Characterization of Polymeric Materials*. New York: Academic Press, 1981
17. Kamal M R. Thermoset characterization for moldability analysis. *Polymer Engineering and Science*, 1974, 14(3): 231–239
18. Zhao L G, Warrior N A, Long A C. A thermo-viscoelastic analysis of process-induced residual stress in fibre-reinforced polymer-matrix composites. *Materials Science and Engineering A*, 2007, 452–453: 483–498
19. Ding A, Li S, Sun J, et al. A thermo-viscoelastic model of process-induced residual stresses in composite structures with considering thermal dependence. *Composite Structures*, 2016, 136: 34–43
20. Takagaki K, Minakuchi S, Takeda N. Process-induced strain and distortion in curved composites. Part I: Development of fiber-optic strain monitoring technique and analytical methods. *Composites Part A: Applied Science and Manufacturing*, 2017, 103: 236–251
21. Zhang G, Wang J, Ni A, et al. Process-induced residual stress of variable-stiffness composite laminates during cure. *Composite Structures*, 2018, 204: 12–21
22. Li D, Li X, Dai J, et al. A comparison of curing process-induced residual stresses and cure shrinkage in micro-scale composite structures with different constitutive laws. *Applied Composite Materials*, 2018, 25(1): 67–84
23. Wang M, Zhang P, Fei Q, et al. Computational evaluation of the effects of void on the transverse tensile strengths of unidirectional composites considering thermal residual stress. *Composite Structures*, 2019, 227: 111287
24. Zhang X X, Wang D, Xiao B L, et al. Enhanced multiscale modeling of macroscopic and microscopic residual stresses evolution during multi-thermo-mechanical processes. *Materials & Design*, 2017, 115: 364–378
25. Maligno A R, Warrior N A, Long A C. Effects of interphase material properties in unidirectional fibre reinforced composites. *Composites Science and Technology*, 2010, 70(1): 36–44
26. Heinrich C, Aldridge M, Wineman A S, et al. Generation of heat and stress during the cure of polymers used in fiber composites. *International Journal of Engineering Science*, 2012, 53: 85–111
27. Yuan Z, Wang Y, Yang G, et al. Evolution of curing residual stresses in composite using multi-scale method. *Composites Part B: Engineering*, 2018, 155: 49–61
28. Qi Y, Jiang D, Ju S, et al. Determining the interphase thickness and properties in carbon fiber reinforced fast and conventional curing epoxy matrix composites using peak force atomic force microscopy. *Composites Science and Technology*, 2019, 184: 107877
29. Bogetti T A, Gillespie J W Jr. Two-dimensional cure simulation of thick thermosetting composites. *Journal of Composite Materials*, 1991, 25(3): 239–273
30. Harte A M, Mc Namara J F. Use of micromechanical modelling in the material characterisation of overinjected thermoplastic composites. *Journal of Materials Processing Technology*, 2006, 173(3): 376–383
31. Ersoy N, Garstka T, Potter K, et al. Development of the properties of a carbon fibre reinforced thermosetting composite through cure. *Composites Part A: Applied Science and Manufacturing*, 2010, 41(3): 401–409
32. Maiarù M, D’Mello R J, Waas A M. Characterization of intralaminar strengths of virtually cured polymer matrix composites. *Composites Part B: Engineering*, 2018, 149: 285–295
33. Minakuchi S, Niwa S, Takagaki K, et al. Composite cure simulation scheme fully integrating internal strain measurement. *Composites Part A: Applied Science and Manufacturing*, 2016, 84: 53–63
34. Bogetti T A, Gillespie J W Jr. Process-induced stress and deformation in thick-section thermoset composite laminates. *Journal of Composite Materials*, 1992, 26(5): 626–660
35. Svanberg J M, Holmberg J A. Prediction of shape distortions. Part II. Experimental validation and analysis of boundary conditions. *Composites Part A: Applied Science and Manufacturing*, 2004, 35(6): 723–734
36. Xia Z, Zhang Y, Ellyin F. A unified periodical boundary conditions for representative volume elements of composites and applications. *International Journal of Solids and Structures*, 2003, 40(8): 1907–1921